 doi:10.20944/preprints202010.0345.v1

Article

Possible early generation of physiological helical flow could benefit the Triflo trileaflet heart valve prosthesis compared to bileaflet valves

Ch. Bruecker*, Qianhui Li

School of Mathematics, Computer Science and Engineering, City, University of London, Northampton Square, London EC1V 0HB, UK.
*Correspondence: Christoph.Bruecker@city.ac.uk

Abstract

Background - Physiological helical flow in the ascending aorta has been well documented in the last two decades, accompanied by discussions on possible physiological benefits of such axial swirl. Recent 4D-MRI studies on healthy volunteers have shown indication of early generation of helical flow, early in the systole and already close to the valve plane.

Objectives - Firstly, the aim of the study is to investigate the hypothesis of premature swirl existence in the ventricular outflow tract leading to already helical flow in the valve plane, and second to investigate the possible impact of two different mechanical valves design on the preservation of this early helical flow and its subsequent hemodynamic consequences.

Methods - We use a pulse duplicator with an aortic arch and High Speed Particle Image Velocimetry to document the flow evolution in the systolic cycle. The pulse-duplicator is modified with a swirl-generating insert to generate early helical flow in the valve plane. Special focus is laid on the interaction of such helical flow with different designs of mechanical prosthetic heart valves, comparing a classical bileaflet mechanical heart valve, the St Jude Medical Regent valve (SJM Regent BMHV) with the Triflo trileaflet mechanical heart valve T2B version (Triflo TMHV).

Results – When the swirl-generator is inserted, a vortex is generated in the core flow demonstrating early helical flow in the valve plane, similar as observed in the recent 4-D-MRI study taken for comparison. For the Triflo trileaflet valve, the early helical flow is not obstructed in the central orifice, similar as in the case of the natural valve. Conservation of angular momentum leads to radial expansion of the core flow and flattening of the axial flow profile downstream in the arch. Furthermore, the early helical flow helps to overcome separation at the outer and inner curvature. In contrast, the two parallel leaflets for the bileaflet valve impose a flow straightener effect, annihilating the angular momentum with negative impact on kinetic energy of the flow.

Conclusion - The results imply better hemodynamics for the Triflo trileaflet valve based on hydrodynamic arguments under the discussed hypothesis. In addition, it makes the Triflo valve a better candidate for replacements in patients with pathological generation of nonaxial velocity in ventricle outflow tract.

Keywords: physiological helical flow, mechanical heart valve prostheses, aorta, PIV, trileaflet

1. Introduction

The flow structures in the aortic arch during the systolic flow pulse show many complex flow features such as vortices, helical streamlines, secondary flows, and retrograde flow regions, all of those regions considerably contributing to the volume-averaged shear load on the blood cells. When a replacement of the natural valve is required, the artificial prosthesis will affect the overall hemodynamic by the alteration of these flow features in size, magnitude and temporal evolution. The more the design of the prostheses differs from the natural valve, the more of such non-physiological changes are expected, which makes the improved design of mechanical heart valves (MHVs) an ongoing research subject of great interest for engineers and clinicians. Despite an increase

Preprints (www.preprints.org) | NOT PEER-REVIEWED | Posted: 16 October 2020 doi:10.20944/preprints202010.0345.v1

development of bioprosthetic surgical valves and transcatheter valves, there is still a need of such a durable valves in younger patient population [10].

To estimate the effect of non-physiological alterations by MHVs, detailed flow studies in simplified mock circuits or CFD simulations are used to obtain the unsteady, 3D flow field data (4D flow field), as illustrated in [1-4] for instance. Those tests are often made with simplified phantoms of the ventricle and the aorta (straight tube), in addition mostly applying uniform inflow conditions. As mentioned in Li et al [5] it is obvious that the valve prosthesis requires to be qualified not only from a hydraulics viewpoint in an isolated environment but also by including the vessel walls into the design and qualification process. This includes the boundary conditions upstream of the valve (diastolic flow in the left ventricle and muscle contraction action) as well as downstream (curved aorta walls, 3D bend). The aortic walls are affected by the complex flow features generated downstream of the valve, causing extra stress loads. It has been reported that high fluctuations of magnitude of the Wall-Shear Stress (WSS) can lead to severe heart diseases [6,7] and affect the aortic wall after implanting artificial heart valves [5,8]. Guzzardi et al [9] have shown that elevated WSS was associated with degradation of the aortic wall. Therefore, they highlighted the importance of investigating whether high velocity jets and high WSS is found in the aorta after implantation of the prosthesis. WSS measurements using micro-pillar sensors reported in Li et al [5] could clearly show considerable differences in the peak oscillations values of WSS generated by different designs of mechanical heart valves (MHVs).

A hitherto not much addressed aspect in flow studies of aortic valve prostheses is the interaction of the valve with possible helical flow features in the aortic arch. Such helical fluid motion is not only relevant for the aortic arch, seemingly it is a common feature in natural flow physiology. Baratchi et al [11] concluded, that the role of helical flow in vessel physiology and pathology is a feature to request a closer look. De Nisco et al. [12] reported an inverse correlation between helical flow and the development of atherosclerotic disease, one example of areas susceptible for atherosclerosis being the inner curvature of the aortic arch. The existence of a right-handed helical flow structure in the ascending aorta is by now a well-acknowledged physiological flow feature [13]. This observation was made possible by the increasing quality of in-vivo velocity measurements such as phase-contrast magnetic resonance imaging (PC-MRI) [14-16]. It goes back to the MRI-study by Kilner et al [17] of the velocity maps in transaortic planes (see Figure 1a), which lets them conclude that the only reasonable interpretation of the combinations of axial and nonaxial velocity patterns is a right-handed helical flow in the upper arch.

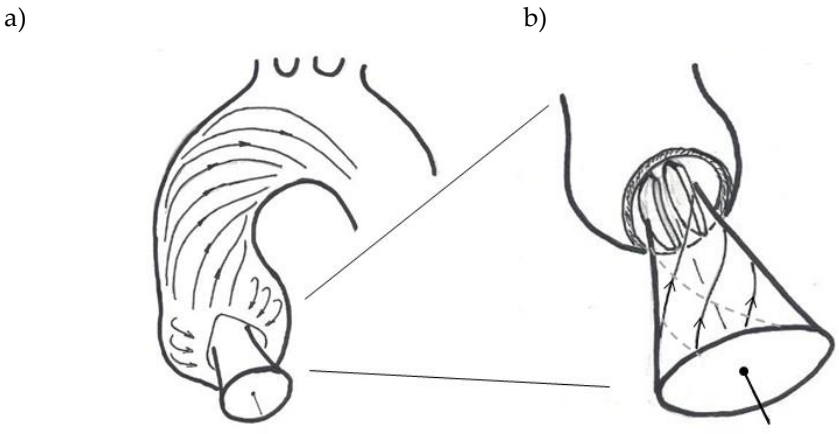

Figure 1: a): adapted sketch from the schematic drawing by Kilner et al [17] to illustrate the evolution of helical flow in the aortic arch; b): hypothesis of the authors with early helical flow generated in the ventricular outlet tract, illustrated by an artistic schematic drawing of a streamtube entering the valve plane. The scene is shown for the case of interaction with an implanted bileaflet MHV.

 doi:10.20944/preprints202010.0345.v1

More recent high-resolution 4D MRI studies reported in [18] indicate that helical flow usually starts already in early-systole in healthy volunteers. Similar, von Spiczak et al [13] found a right-handed vortex arising in the ascending aorta early in systole and propagating to the aortic arch with peak vorticity values reached in mid systole. As more and more 4D MRI data show a right-handed swirling flow early in systole, also directly above the valve, this flow feature probably is not only induced by the downstream curvature of the arch. The hypothesis introduced herein and illustrated in Figure 1b is as follows: the right-handed helix in the ascending aorta may partly being fed *from* ***early swirl in the ventricle outflow tract*** *entering the aortic arch*. The following arguments led us to this hypothesis:

- *The convective nature of the swirl growth* - the recent 4D-MRI studies in [13,18] observed that the swirl propagates from the valve plane further into the aortic arch with progress of the systolic cycle.
- *Angular momentum generated during the filling procedure of the left ventricle*, which does not completely cease until the beginning of the systole - it is documented in previous research that a vortex ring or a tumble vortex [19] is generated in the filling phase. The flow in the ventricular outflow tract therefore has a non-axial component.
- *The helical ventricle contraction* - it is reasonable to assume that the left ventricle contraction re-orients the spin-vector of existing angular momentum into the ejection direction, causing a swirl component of the axial flow. This is supported eventually by the helical wave-type contraction pattern and the helical ventricular myocardial band [20,21].
- *The bathtub vortex effect* - any weak swirl in the convergent outflow tract is strengthened when the flow accelerates to the valve plane. This is due to conservation of angular momentum, similar to a bathtub vortex when draining through a small orifice. In their original paper, Kilner et al [17] also mentioned that the existence of a possible helical flow in the ventricular outflow tract could not be excluded, a definite conclusion was not possible because of the limits of resolution power of MRI.

Our study aims are two-fold: firstly, we introduce a modified in-vitro pulse-duplicator which generates early helical flow in the valve plane. This allows us to compare the evolution of axial swirl in the valve plane of the aortic arch over the systolic cycle and to compare the data with most recent data from 4D-MRI, addressing the arguments of the hypothesis. Secondly, we want to understand the interaction of early helical flow with different designs of mechanical heart-valve prostheses and the hydrodynamic consequences thereof, an example being a bileaflet valve as illustrated in the sketch in Figure 1b. To achieve high resolution in both space and time, High-Speed Particle-Image Velocimetry (HS-PIV) measurements are carried out to improve our understanding of unsteady and pulsatile flow phenomena linked to the interaction of the swirling flow with the valve.

2. Materials and Methods

2.1. Pulse duplicator

An in-house built pulse duplicator is used for the flow studies herein, similar to the one used in our previous study [5]. The core components are a programmable linear actuator with a piston at its axle, which is connected to a fluid tank that contains a transparent phantom model of an aortic arch (flat curved tube). The total pressure head can be adjusted by the pressure within the tank. Different flow resistances at the outlets can be adjusted by inserting nozzles into the openings of the phantom. A sketch of the experimental setup is shown in Figure 2a. The imposed flow profile for the current studies is given in Figure 2b, which shows a typical systolic flow pulse with maximum velocity reached at about 30% of the systolic cycle.

Preprints (www.preprints.org) | NOT PEER-REVIEWED | Posted: 16 October 2020 doi:10.20944/preprints202010.0345.v1

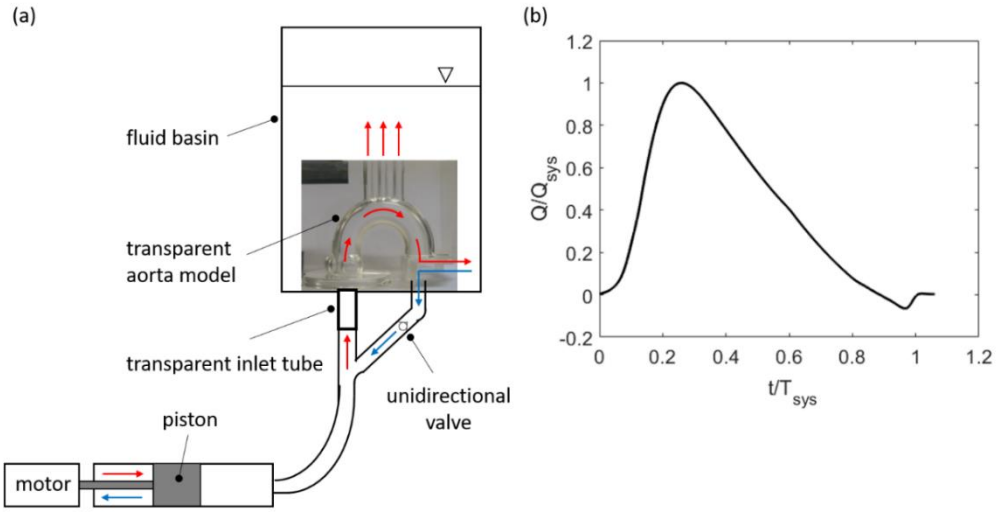

Figure 2: Sketch of the pulse duplicator and the flow profile in the systolic phase.

The systolic heartbeat with duration of T_{sys}=386 ms is characterised by an accelerated flow phase from 0 to $0.2T_{sys}$, then a peak systole phase from $0.2T_{sys}$ to $0.4T_{sys}$, followed by a decelerated flow phase from $0.4T_{sys}$ to $0.8T_{sys}$, and finally the valve closure phase from $0.8T_{sys}$ to T_{sys}. At the peak of the flow, the peak inlet velocity reaches a value of U_P = 0.95 m/s. The mean velocity averaged over the complete beat cycle amounts to U_m = 0.19 m/s. The non-dimensional physical parameters of the flow can be represented by the Reynolds number eq. (1), Strouhal number eq. (2) and Womersley number eq. (3):

$$Re_P = \frac{\rho U_P D_A}{\mu} \tag{1}$$

$$St = \frac{D_A}{2}\frac{f}{(U_P - U_m)} \tag{2}$$

$$\alpha = \frac{D_A}{2}\sqrt{\frac{2\pi f \rho}{\mu}}, \tag{3}$$

For a heartbeat rate f of 1.15 Hz (70 BPM), the Reynolds, Strouhal, and Womersley numbers are $Re_P = 5340$, $St = 0.019$ and $\alpha = 16$, respectively. These values of the non-dimensional physical parameters are similar to those that have been observed in the in-vivo experiment of the healthy aorta performed among 30 volunteers by Stalder et al [22]. This indicates that the flow conditions used in the present study are representative for the natural flow situation.

The geometry of the aorta model is taken from Vasava et al [23], who simplified the geometry derived from a three-dimensional reconstruction of a series of two-dimensional slices obtained in vivo using CT scan imaging on a human aorta by Shahcheraghi et al [24]. The diameter of the aorta is D_A = 25 mm, and the MHVs are then sized accordingly. The 180° curved bend representing the aortic arch with sinuses of Valsalva (SOV) has a planar symmetry plane (crossing the left sinus in the middle), which eases the fabrication of the model. The details of the casting process has been described in detail in our previous study [5].

2.2. Heart valve prostheses

The effect of helical flow is studied for two different valve prostheses, one classical bileaflet mechanical heart valve, the St. Jude Medical Regent valve (SJM Regent BMHV) valve from Abbott Laboratories, U.S.A) and the Triflo trileaflet mechanical heart valve T2B version (Triflo TMHV) from Novostia SA, Switzerland, both size 25 mm (tissue annulus diameter) with an almost identical inner diameter (D_A = 23.2 mm for the Triflo TMHV versus D_A = 23.0 mm for the SJM Regent TMHV). The

Preprints (www.preprints.org) | NOT PEER-REVIEWED | Posted: 16 October 2020 doi:10.20944/preprints202010.0345.v1

SJM Regent BHMV is a widely used MHV which was introduced in the market in 1978. The Triflo TMHV consists of three leaflets that open to form a central orifice for the blood to flow through and three side orifices jets. The Triflo TMHV has been studied over the years in vitro [25-27], and its in-vivo performance has successfully been evaluated in animal studies [28]. As the design more closely resembles the natural aortic valves, it is assumed to have a better hemodynamic performance. A circular tube-segment is also used as kind of an open valve without any leaflets to obtain the "undisturbed" flow situation in the aortic valve plane. Those data are taken as reference.

The arrangement of the heart valves is as displayed by the top view as shown in Figure 3, including the reference case, i.e. the open circular orifice nozzle configuration, SJM Regent BMHV configuration and Triflo TMHV configuration. The thin-walled circular orifice nozzle with an outer diameter of 25 mm and an inner diameter of 24.6 mm is inserted in the valve plane, which covers the SOV, allowing the bulk flow to smoothly enter through the step-free inlet into the bend. The BMHV and the Triflo TMHV are orientated, in both cases, such that one leaflet is facing the sinus bulb at the outer aortic wall. For the Triflo TMHV, the remaining leaflets then face the direction of the other sinus bulbs. While the other leaflet of the BMHV is in the middle of sinus bulbs, facing to the inner aortic wall.

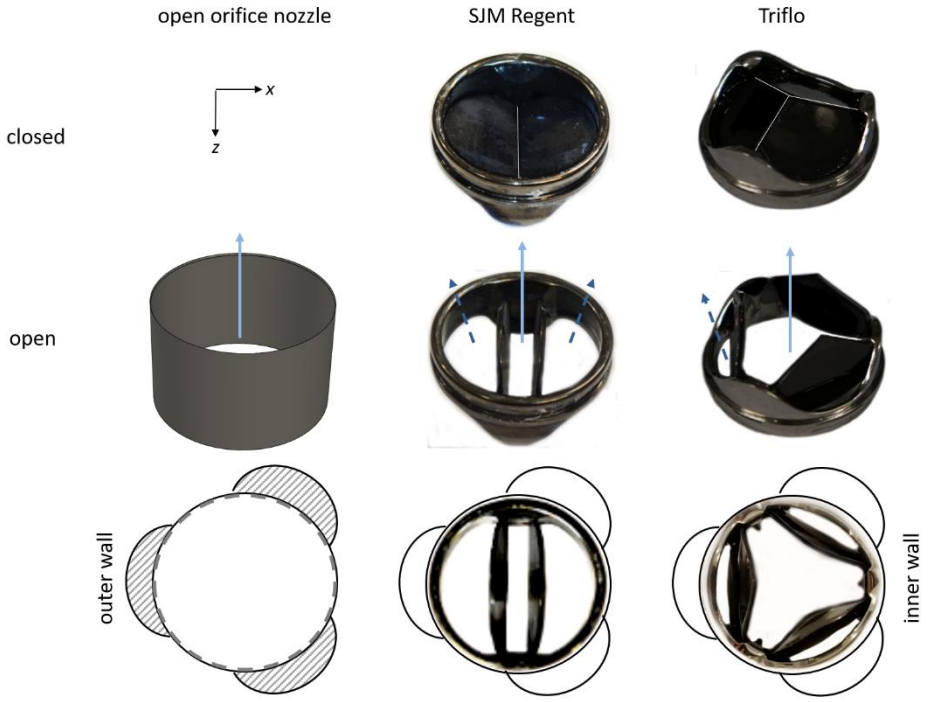

Figure 3: Tested heart-valve prostheses and their orientation within the aorta phantom. Left column: an open orifice nozzle with circular cross-section and thin wall to cover the sinuses, forming a continuous smooth bend. Middle column: SJM Regent BMHV size 25 mm, with the leaflets in a fully open position (opening angle: 85°) and in the closed position (closed angle 25°). Right column: Triflo TMHV size 25 mm with the leaflets in the fully open position (opening angle 90°) and in the closed position (closed angle 40°). The solid arrow marks the center orifice jet, and the dashed arrows mark the side orifice jets.

2.3. Optical flow mapping

The transparent aorta phantom is then placed at the bottom of the transparent basin (width/depth: 190 mm, height: 500 mm) as shown in Figure 4, and subsequently filled with a glycerine-water solution (58/42 % by mass, density $\rho = 1140$ kg·m^{-3}, dynamic viscosity $\mu = 5$ mPa·s at the temperature of 38°C, refractive index 1.41). The refractive index of the glycerine-water matches that of the silicone model such that there is undisturbed optical access into the inner of the aorta. It

Preprints (www.preprints.org) | NOT PEER-REVIEWED | Posted: 16 October 2020 doi:10.20944/preprints202010.0345.v1

must be noted here that the working fluid in the present study has a Newtonian behaviour, which differs from the non-Newtonian behaviour of blood.

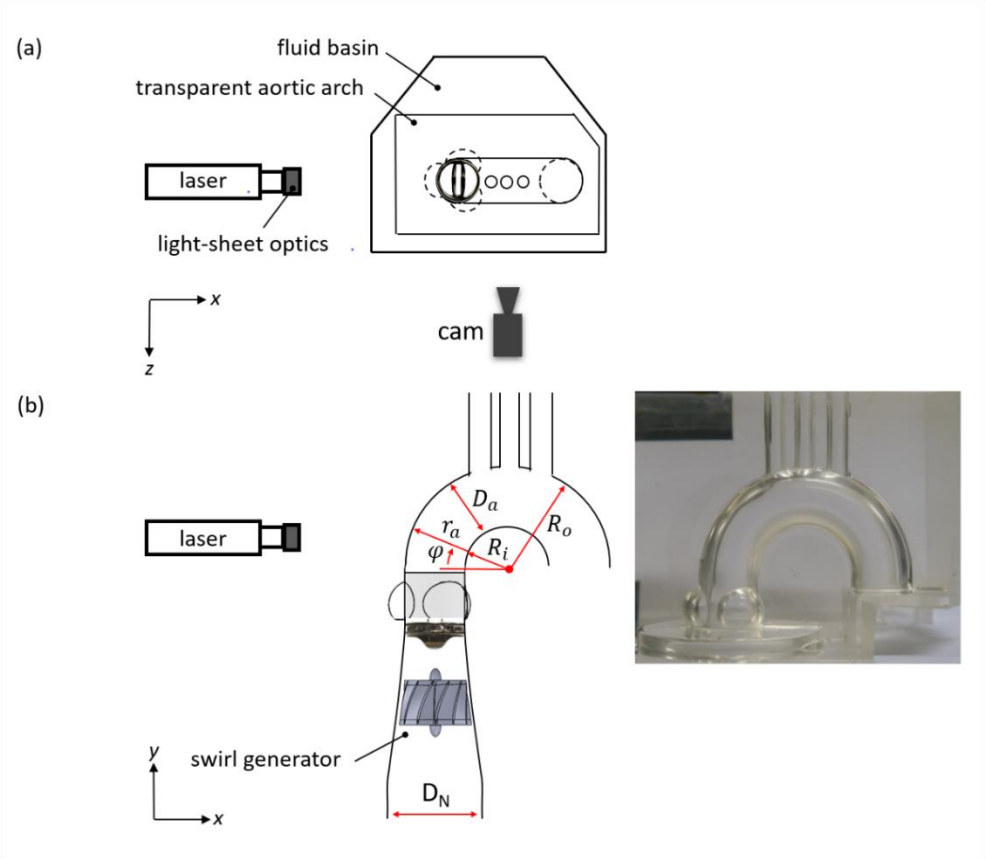

Figure 4: Details of the aorta phantom (incl sinuses and brachiocephalic arteries) with additional inlet swirl generator module upstream of the aortic valve plane. The converging inlet nozzle has a initial diameter D_N=40mm and length of $2D_N$, in which the swirl generator with an exit angle of 30° is inserted. For optical flow diagnostics, the transparent model is placed in a liquid container filled with the working fluid. This allows unobstructed view into the inner flow and velocity measurements using the method of HS-PIV. The measurement plane can be arranged in the horizontal cross-section above the valve plane and in the vertical symmetry-plane of the bend.

2.4. High-Speed Particle Image Velocimetry

The PIV system is the same as used in our previous study [5]. Small tracer particles (fluospheres, mean diameter d_p =30 µm, Dantec Dynamics, density ρ_p = 1040 kg·m^{-3}) are added to the working liquid for the HS-PIV measurements. The Stokes number for these particles is $Stk = \tau U_P/d_p \approx 0.33 \ll 1$, where the peak inlet velocity (U_P=0.95 m/s) is taken as the velocity scaler and the characteristic time scale is $\tau = \rho_p\, d_p^2/(18\mu) \approx 10\ \mu s$ [29]. This indicates that particles are able to follow the streamlines closely. A continuous wave Argon-Ion laser (Raypower 5000, 5 W power at λ = 532 nm, Dantec Dynamics) is used as an illumination source. The output laser beam is approximately 1.5 mm in diameter and is further expanded into a sheet illuminating the symmetry plane of the aorta. Full format recordings of the flow in the AAo are taken with a high-speed camera (Phantom Miro 310, Ametek, 576 × 768 px^2 recording at 7200 fps) equipped with a lens (Tokima Macro f= 100mm, F 2.8) giving a field of view of 57.6 x 76.8 mm^2. Furthermore, HS-PIV measurements are taken in the radial cross-section above the aortic bulb with the camera looking from top. Axial vorticity is then calculated from the velocity field in this plane by taking the curl of the velocity vector field at each data point. The unit of vorticity is given as s^{-1}.

Preprints (www.preprints.org) | NOT PEER-REVIEWED | Posted: 16 October 2020 doi:10.20944/preprints202010.0345.v1

3. Results

3.1. Outlet flow with swirl

The hypothesis of generation of early helical flow in the valve plane has been investigated based on comparison of our results with published data, the most relevant being the recent study from von Spiczak et al [13] using high-resolution phase-constrast MRI on healthy volunteers. As we cannot reproduce the data for a natural valve at a cross-section above the aortic bulbs, we use here the open orifice (see Fig. 3 left) in the pulse-duplicator, which represents approximately a fully open natural valve. The opening phase is not considered herein. Citing their results for healthy volunteers [13] (p. 12): "*clock-wise CW rotational flow is developed during early systole. It could be observed first in ROI 0 and 1, which were located directly above the aortic bulb and in the ascending aorta, respectively (ROI 0: minimal vorticity = -166.4±86.4 s^{-1} at 12% of cardiac cycle and ROI 1: -183.6±65.3 s^{-1} at 16%). Thereupon, rotational flow propagated to the more distal ROIs 2, 3, and 4 with minimum values seen in mid systole (ROI 2: -240.1±45.2 s^{-1} at 16%, ROI 3: -229.2±50.0 s^{-1} at 20%, and ROI 4: -201.6±92.7 s^{-1} at 16%)*". In addition, as mentioned in [13] (p. 1): "*strength, elongation, and radial expansion of 3D vortex cores escalated in early systole, reaching a peak in mid systole (strength = 241.2±30.7 s^{-1} at 17%, elongation = 65.1±34.6 mm at 18%, expansion = 80.1±48.8 mm^2 at 20%), before all three parameters similarly decreased to overall low values in diastole*." The HS-PIV measurements in the radial cross-section above the aortic bulb correspond to their Region of Interest (ROI) ROI 1. The velocity data obtained in this plane in the experiments allow to quantify the axial vorticity (the spin-vector of the helical flow is in axial flow direction). As in agreement with their definition, negative values of axial vorticity stand for clockwise (CW) fluid motion. This direction is in the same direction as the physiological helix. Figure 5 shows the experimentally obtained contours of the axial vorticity overlaid on the cross-sectional vector field. The core of the CW vortex is well seen by the region of concentrated negative vorticity (in blue). An indication of the diameter is given by the circle which is drawn along the radius of maximum tangential velocity (maximum value of about 0.5 m/s). This diameter is about 10 mm, which yields a core "expansion" of 75 mm^2, well in the range reported by von Spiczak et al [13]. Note that the core is somewhat dislocated away from the centre towards the inner curvature because of the upstream effect of the arch.

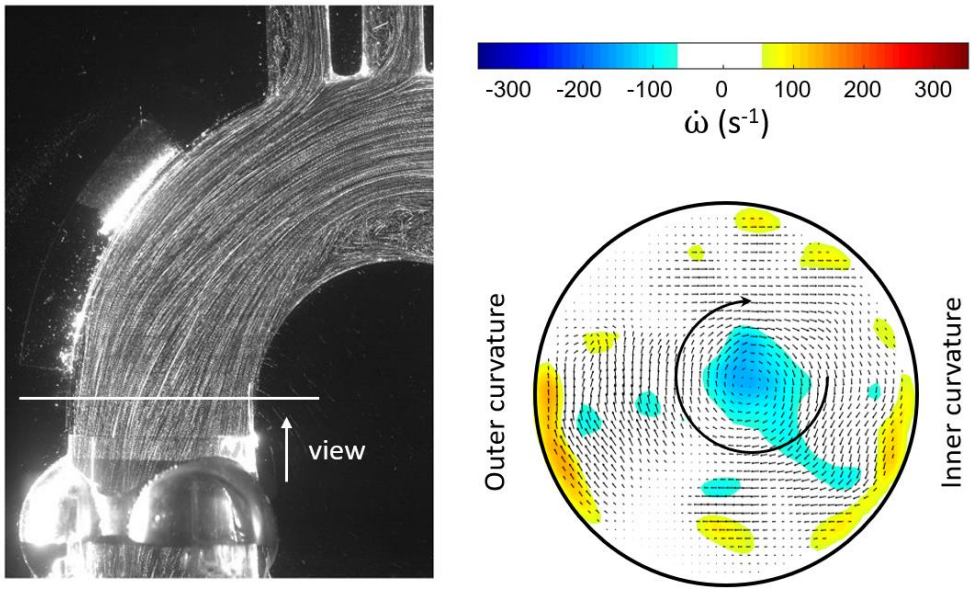

Figure 5: Circular orifice flow with inlet swirl at peak systole observed in the pulse duplicator. Left: Pathlines at peak systole shown by multi-exposure images in the light-sheet crossing the center plane, right: velocity field in the cross-section above the bulb indicating the vortex core (color levels indicate

Preprints (www.preprints.org) | NOT PEER-REVIEWED | Posted: 16 October 2020 doi:10.20944/preprints202010.0345.v1

axial vorticity, the inner circle shows the diameter of the vortex core).

An important benefit of the HS-PIV recordings is the potential to use the images also for creation of a flow visualization picture showing the flow path lines. The flow path lines displayed in Figure 5 let recognize the difficulty to capture the helical character of the flow just from this information. What looks like a rather parallel flow with little tilt towards the inner curvature is the results from high axial velocity of order of 1.5 m/s in the core, while considerable circumferential velocity of 30% of the peak axial velocity exists simultaneous. Maximum visibility of the helical flow nature would only be possible by starting virtual path lines along the circle in Figure 5 right as this is the location of maximum circumferential velocity in this cross-section. This observation supports also the methodology of a rigorous quantitative approach from the MRI data as done by von Spiczak et al [13] to extract fundamental quantities such as vortex core size, strength and temporal evolution of those quantities in different regions of interest (ROI).

Additional information is given by the temporal evolution of the peak negative value of axial vorticity in the core. The experimental data are again compared to the values from von Spiczak et al [13]. Both plots show a similar profile with early generation of a core region of concentrated axial vorticity. Peak minimum values are reached about mid systole between 0.4 - 0.5T_{sys}. The similar trend in the temporal evolution near to the valve plane hints that there is reasonable support to our hypothesis that early swirl could have been generated in the ventricular outflow tract and been transported into the ascending aorta. Note that possible swirl in the ventricular outflow tract may have been overlooked as it is only intensified when accelerated towards the valve orifice, similar as a bathtub vortex when draining into a small orifice (due to conservation of angular momentum in a convergent flow tube).

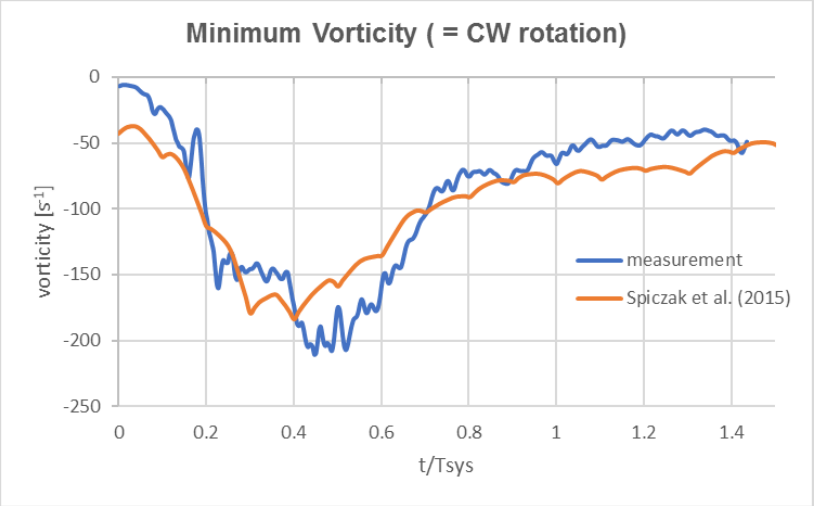

Figure 6: Peak negative vorticity value in the vortex core at the cross-section above the bulb in the Pulse Duplicator compared to the 4D MRI flow data of von Spiczak et al [13] in ROI 1 at a similar position. Note the early development of the vortex in the plane above the bulb.

3.2. Helical flow Interaction with MHV

Further on, HS-PIV was used to study the influence of early helical flow on the hydrodynamics of MHVs in the ascending aorta, comparing the Triflo TMHV with the SJM Regent BMHV. For better visibility of the effect of early helical flow, we compare the situation with/without swirl generator inserted. The velocity fields in the centre plane (symmetry plane of the phantom) are shown for three selected instants in the peak systole, first as color-coded contours of constant axial velocity and secondly also as profiles of the same component of the velocity vector at different angles of the arch.

For the Triflo TMHV (see figure 7), in the early systole, the overall flow pattern in the centre-plane in the arch is not much affected by the presence of the swirl. Later in the systole, a difference is clearly visible in the lateral boundary of the core jet. For the no-swirl situation, the core penetrates

Preprints (www.preprints.org) | NOT PEER-REVIEWED | Posted: 16 October 2020 doi:10.20944/preprints202010.0345.v1

the aorta in a straight way and separation is observed at the outer and inner curvature wall further downstream. For the swirl-case, the core contains angular momentum, which results in a radial pressure gradient (pressure minimum at the centre). When the central jet leaves the valve region, it immediately spreads radially and the flow attaches to both, the inner and the outer curvature wall. Consequently, the core widens and the velocity profile gets a more homogeneous plateau in the central region. The radial spread also re-energizes the flow in the near-wall regions, which is well-seen by the increased axial velocities near the walls compared to the no-swirl case (marked as the circular region in Figure 7). Therefore, the boundary layer flow in the swirl case is more resistant to adverse pressure gradients, thereby overcoming the risk of flow separation. Indeed, the swirl case shows only a marginal case of separation at the inner wall compared to the no-swirl case. Another observation is a much stronger recirculation within the sinuses for the swirl-case. This supports an early begin of closure of the leaflets of the Triflo TMHV at $0.77T_{sys}$ compared to $0.8T_{sys}$ in the no-swirl case (no early helical flow).

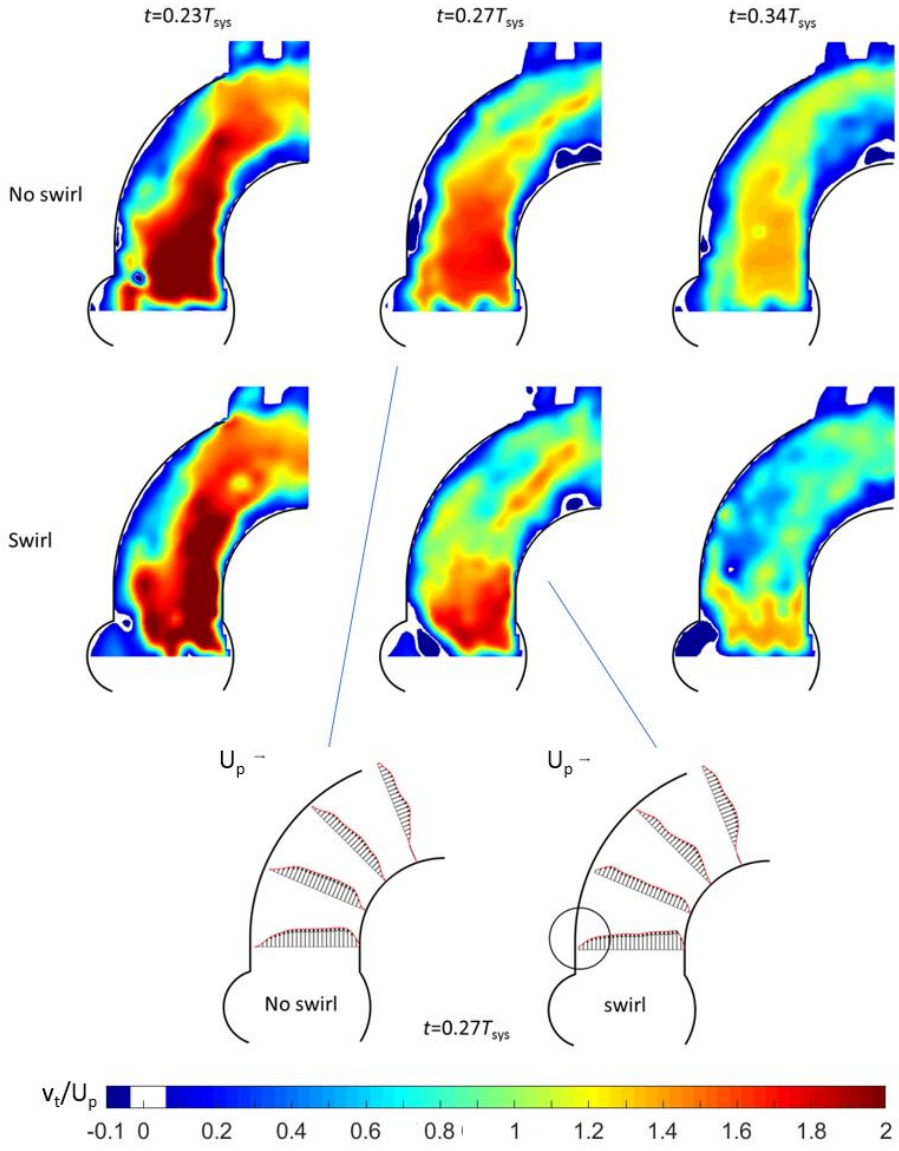

Figure 7: HS-PIV visualization of the flow evolution in the center plane of the aorta phantom for the Triflo valve with/without inlet swirl in the Pulse Duplicator: Color-coded contours of constant axial velocity (top) and axial velocity profiles in the center plane.

Preprints (www.preprints.org) | NOT PEER-REVIEWED | Posted: 16 October 2020 doi:10.20944/preprints202010.0345.v1

Results for the BMHV are given in Figure 8. As for the Triflo TMHV, in the early systole the flow in the centre-plane in the arch is not much affected by the presence of the swirl. For the no-swirl situation, one can see a clear indication of the three jets, the two side-orifice jets and the core jet between the leaflets at the centre of the valve. A striking effect of the swirl is the drastic reduction of the velocity in the central jet. This reduction of the axial velocity can be explained by the existence of concentrated streamwise vorticity in the core when it is interacting with the divergent flow channel formed between both leaflets. The flow passage between the two leaflets is comparable to a swirling flow through a diffusor with opening angle of 5-10°. As known from the phenomenon of vortex breakdown, this causes a reduction of the axial velocity predominantly at the centre, sometimes even leading to flow reversal along the swirl axis [30] [31]. Due to the velocity deficit in the centre, more flow is going into the side-orifice jets, seen by the somewhat larger axial velocities therein. Both jets attach to the nearby walls, increasing locally in the attachment location the WSS values. While the swirl has a positive effect on the retarded region at the inner curvature of the aorta, it has a negative effect on the flow along the outer curvature as the large blue-colored region of near-stagnant flow has grown in size along the curve.

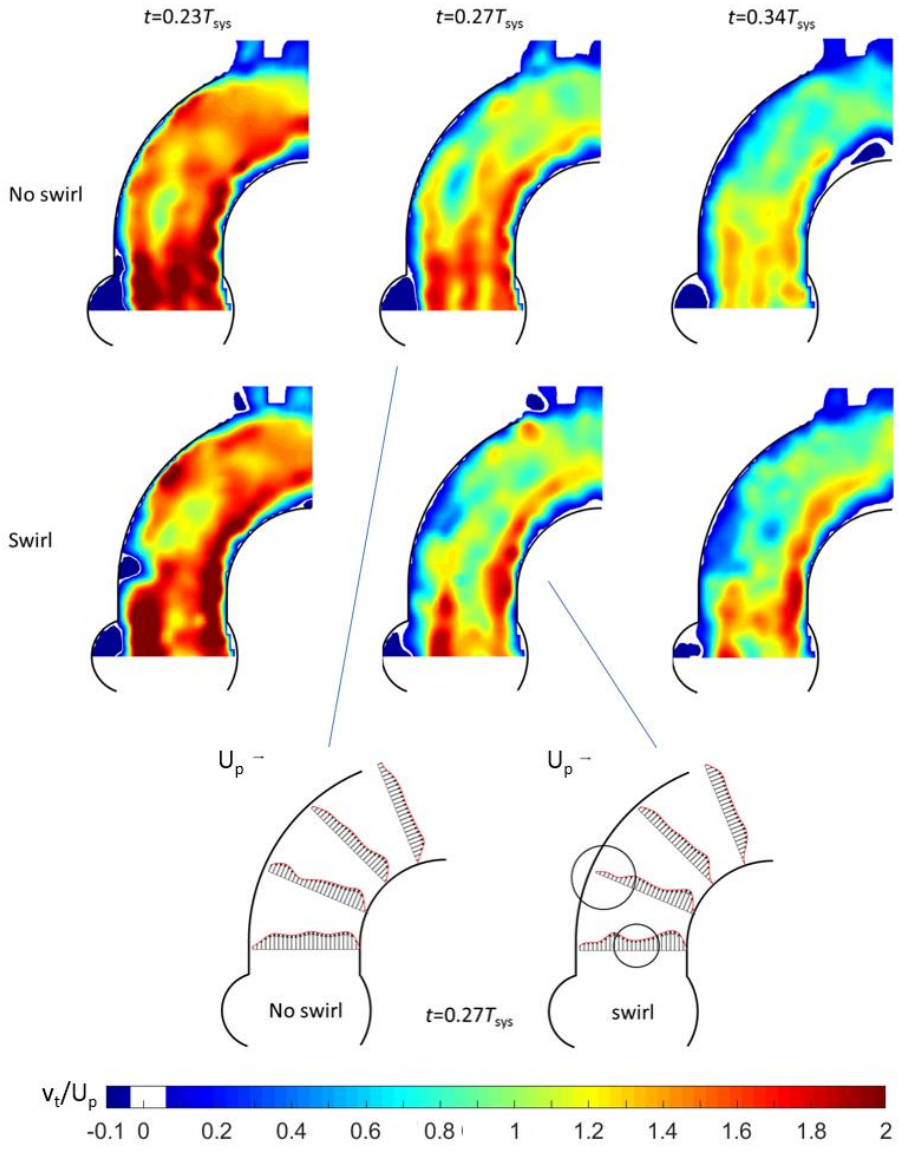

Figure 8: HS-PIV visualization of the contours of axial velocity magnitude (top) and axial velocity profiles in the center plane during systole in the Pulse Duplicator for BMHV.

 doi:10.20944/preprints202010.0345.v1

4. Discussion

The present work investigates for the first time the influence of early generation of helical flow in the valve plane on the hydrodynamics of different types of mechanical heart valve prosthesis. Although the phantom of the aortic arch is curved only in one plane, we could see beneficial effects of the early helical flow on the generation and growth of flow separation at the inner curvature of the arch. As the Triflo TMHV allows the core flow to convect through the valve pane and further downstream without objecting the tangential velocity, angular momentum in the flow is conserved. Downstream of the valve, the radial pressure gradient in the core leads to a radial expansion of the core region over the complete radial cross-section of the ascending aorta. This reduces the peak velocities in the core jet and the shear-stresses in the shear layer between the core jets and the annular region near the wall. In addition, the recirculation flow in the sinuses is enhanced, supporting the early begin of leaflet motion in the closing phase at $0.77T_{sys}$ in the swirl case compared to $0.8T_{sys}$ in the no-swirl case (no early helical flow).

The impact of early helical flow in the valve plane on the flow downstream of the BMHV is seen by a seemingly change of flow-partitioning between the three jets, the two side orifice jets and the center jet. The latter shows reduced velocity in the center while the side orifice jets become stronger, therefore the valve guides a higher amount of fluid through the side orifices compared to the center. The bileaflet valve with its leaflets oriented in axial direction works in principle as a flow-straightener by objecting the nonaxial flow components (see Fig 1b). The nearly parallel planes of both leaflets guide the flow in axial direction, similar as the guide-vanes of a stator known in turbomachinery. Such a device is usually implemented at the exit of a flow pump to convert kinetic energy of the swirling flow into higher pressure. This is achieved by reducing the tangential velocity direction downstream to zero in a smooth way using curved vanes. However, a larger energy loss (total pressure loss) occurs if the guide-vanes are planar and parallel to the axial flow, similar as the leaflets in the BMHV. Therefore, under the conditions of early generation of helical flow entering the valve plane, this effect is to cause an additional hydrodynamic pressure drop of the BMHV that the left ventricle needs to overcome to eject the same amount fluid in the systolic pulse compared to the situation of the natural valve. This is contrary to the herein described Triflo TMHV, which has per-se a design where the leaflets open the central area without obstructing bodies. Therefore, the core of the swirl flow can penetrate through the valve with conservation of angular momentum.

5. Conclusion

The present study has investigated the hypothesis of early generation of helical flow in the valve plane of the aortic arch and its consequences on the hydrodynamics of MHVs and the flow in the arch. Firstly, we see the hypothesis supported by the following observations:

- good agreement of the measured axial vortex in the valve plane of the aortic arch in the Pulse-Duplicator with recent published data of 4D MRI studies in the aortic arch of healthy volunteers.
- In the Pulse Duplicator, the axial vortex is generated with a swirl-generator inserted into the inlet tube upstream of the valve while in the MRI data it is a result of the complex flow evolution during left ventricular ejection into the aortic arch. The near overlap of the data in magnitude and temporal evolution between our experiment and the MRI data suggest that early generation of helical flow in the valve plane indeed could originate from swirl in the ventricular outflow tract, which is convected into the arch.
- As mentioned already by Kilner et al [17], the tortuous, S-shaped form of the vertebrate heart causes multidirectional intracardiac flow patterns, which may cause efficient directional exchange of energy between muscle and blood in the ejection. From any reconstructions of path lines patterns alone it is difficult to detect such a helical motion in the valve plane. Rather, quantifying the regions of concentrated axial vorticity in the cross-sectional planes of the ventricle

and arch is necessary, similar to what has been done herein for the HS-PIV measurements and by von Spiczak et al [13] in their MRI data.

Secondly, with the above given reasonable arguments of the existence of early generation of helical flow in the valve plane, the hydrodynamics of MHVs requires a closer look with regards to this effect on different aspects of the valve design. With existence of early generation of helical flow in the valve plane the following conclusions can be drawn based on the results and hydrodynamic arguments:

conservation of angular momentum for the Triflo TMHV - it preserves angular momentum in the core flow, which helps to re-distribute and expand the core flow downstream of the valve towards the walls of the aortic arch, reducing the potential of flow separation in the inner and outer curvature of the arch. Therefore the physiological helical flow is preserved throughout the valve plane and the aortic arch. This might also have consequences on the distribution of existing micro-bubbles in the flow. Those gas bubbles tend to migrate to the center of the swirling flow, where the pressure minimum is. Consequently, micro-bubbles entering the arch remain in the centre of the helical flow and therefore there is less risk to enter the barocerebral arteries at the apex of the arch.

flow straightener effect for the bileaflet BMHV - flow partitioning between the side-orifices and center orifice changes due to the complex interaction of the swirling flow with the leaflets, which act as guide vanes. The axially oriented parallel leaflets obstruct nonaxial flow components, therefore the conversion from helical flow to axial flow does not happen in a smooth, loss-free way within the vane channels. The consequence is a drop of kinetic energy (total pressure loss) of the flow when passing the valve. Therefore, the required workload of the left ventricle for fluid ejection through the Triflo TMHV is expected to be lower than that for a bileaflet valve, as the helical flow is preserved.

Overall, the observations under the given hypothesis give more reasons for a superior hemodynamics of the Triflo TMHV against bileaflet valves on its own. Further studies are planned with the latest version of the Triflo valve in the Pulse Duplicator and in 4D-MRI studies of an isolated pig-heart. In the latter, special focus will be to gain more detailed information of the flow in the ventricular outflow tract to test the hypothesis under realistic conditions of geometrical and physiological conditions of a beating heart. In addition, the experiments in the Pulse-Duplicator will be repeated with an in-house developed Scanning PIV technique to obtain the 3D volumetric velocity field instantaneously in the whole arch.

Supplementary Materials: The following are available online at www.mdpi.com/xxx/s1, Figure S1: title,

Author Contributions: Conceptualization, Ch. Bruecker; methodology, Ch. Bruecker and Qianhui Li; software, Ch. Bruecker and Qianhui Li; validation, Ch. Bruecker and Qianhui Li; formal analysis, Ch. Bruecker; investigation, Ch. Bruecker; resources, Ch. Bruecker; data curation, Ch. Bruecker and Qianhui Li; writing—original draft preparation, Ch. Bruecker and Qianhui Li; writing—review and editing, Ch. Bruecker and Qianhui Li; visualization, Qianhui Li; supervision, Ch. Bruecker; project administration, Ch. Bruecker; funding acquisition, Ch. Bruecker. All authors have read and agreed to the published version of the manuscript.

Funding: This research was funded by BAE Systems and the Royal Academy of Engineering (grant number RCSRF1617\4\11), and German Research Foundation (grant number DFG 1494/32-1).

Acknowledgments: The position of Professor Christoph Bruecker is sponsored by BAE System and the Royal Academy of Engineering (RCSRF1617\4\11), which is gratefully acknowledged herein. The German Research Foundation supported PhD Qianhui Li (DFG 1494/32-1), which is also gratefully acknowledged. The authors would also like to express our thanks to the Helmholtz Institute of RWTH Aachen University, Germany, for providing the SJM Regent valve and Novostia Switzerland for providing the Triflo valve (T2B version) used in this project.

 doi:10.20944/preprints202010.0345.v1

Conflicts of Interest: CB has conducted consultancy advise for Novostia on the topic of reviewing fluid mechanical results of new versions of the Triflo valve from external partners. The remaining authors have no conflicts of interest to declare.

References

1. Dasi, L.; Ge, L.; Simon, H.; Sotiropoulos, F.; Yoganathan, A. Vorticity dynamics of a bileaflet mechanical heart valve in an axisymmetric aorta. *Physics of Fluids* **2007**, *19*, 067105.
2. De Tullio, M.D.; Cristallo, A.; Balaras, E.; Verzicco, R. Direct numerical simulation of the pulsatile flow through an aortic bileaflet mechanical heart valve. *Journal of Fluid Mechanics* **2009**, *622*, 259-290.
3. Barannyk, O.; Oshkai, P. The influence of the aortic root geometry on flow characteristics of a prosthetic heart valve. *Journal of biomechanical engineering* **2015**, *137*, 051005.
4. Borazjani, I.; Ge, L.; Sotiropoulos, F. High-resolution fluid–structure interaction simulations of flow through a bi-leaflet mechanical heart valve in an anatomic aorta. *Annals of biomedical engineering* **2010**, *38*, 326-344.
5. Li, Q.; Hegner, F.; Bruecker, C.H. Comparative study of wall-shear stress at the ascending aorta for different mechanical heart valve prostheses. *Journal of biomechanical engineering* **2020**, *142*.
6. Walker, P.G.; Yoganathan, A.P. In vitro pulsatile flow hemodynamics of five mechanical aortic heart valve prostheses. *European journal of cardio-thoracic surgery* **1992**, *6*, S113-S123.
7. Marsden, A.L.; Bazilevs, Y.; Long, C.C.; Behr, M. Recent advances in computational methodology for simulation of mechanical circulatory assist devices. *Wiley Interdisciplinary Reviews: Systems Biology and Medicine* **2014**, *6*, 169-188.
8. Arzani, A.; Shadden, S.C. Wall shear stress fixed points in cardiovascular fluid mechanics. *Journal of Biomechanics* **2018**.
9. Guzzardi, D.G.; Barker, A.J.; Van Ooij, P.; Malaisrie, S.C.; Puthumana, J.J.; Belke, D.D.; Mewhort, H.E.; Svystonyuk, D.A.; Kang, S.; Verma, S. Valve-related hemodynamics mediate human bicuspid aortopathy: insights from wall shear stress mapping. *Journal of the American College of Cardiology* **2015**, *66*, 892-900.
10. David, T. How to decide between a bioprosthetic and mechanical valve. *Canadian Journal of Cardiology* **2020**.
11. Baratchi, S.; Chen, Y.-C.; Peter, K. Helical flow: A means to identify unstable plaques and a new direction for the design of vascular grafts and stents. *Atherosclerosis* **2020**, *300*, 34-36.
12. De Nisco, G.; Kok, A.M.; Chiastra, C.; Gallo, D.; Hoogendoorn, A.; Migliavacca, F.; Wentzel, J.J.; Morbiducci, U. The atheroprotective nature of helical flow in coronary arteries. *Annals of biomedical engineering* **2019**, *47*, 425-438.
13. von Spiczak, J.; Crelier, G.; Giese, D.; Kozerke, S.; Maintz, D.; Bunck, A.C. Quantitative analysis of vortical blood flow in the thoracic aorta using 4D phase contrast MRI. *PLoS One* **2015**, *10*, e0139025.
14. Potters, W.V.; Marquering, H.A.; VanBavel, E.; Nederveen, A.J. Measuring wall shear stress using velocity-encoded MRI. *Current Cardiovascular Imaging Reports* **2014**, *7*, 9257, doi:https://doi.org/10.1007/s12410-014-9257-1.
15. Markl, M.; Wallis, W.; Harloff, A. Reproducibility of flow and wall shear stress analysis using flow ‐ sensitive four ‐ dimensional MRI. *Journal of Magnetic Resonance Imaging* **2011**, *33*, 988-994, doi:https://doi.org/10.1002/jmri.22519.
16. Papathanasopoulou, P.; Zhao, S.; Köhler, U.; Robertson, M.B.; Long, Q.; Hoskins, P.; Yun Xu, X.; Marshall, I. MRI measurement of time ‐ resolved wall shear stress vectors in a carotid bifurcation model, and comparison with CFD predictions. *Journal of Magnetic Resonance Imaging* **2003**, *17*, 153-162, doi:https://doi.org/10.1002/jmri.10243.
17. Kilner, P.J.; Yang, G.Z.; Mohiaddin, R.H.; Firmin, D.N.; Longmore, D.B. Helical and retrograde secondary flow patterns in the aortic arch studied by three-directional magnetic resonance velocity mapping. *Circulation* **1993**, *88*, 2235-2247.
18. Ebel, S.; Dufke, J.; Köhler, B.; Preim, B.; Behrendt, B.; Riekena, B.; Jung, B.; Stehning, C.; Kropf, S.; Grothoff, M. Automated Quantitative extraction and Analysis of 4D flow Patterns

in the Ascending Aorta: An intraindividual comparison at 1.5 T and 3 T. *Scientific reports* **2020**, *10*, 1-13.

19. Dabiri, J.O.; Gharib, M. The role of optimal vortex formation in biological fluid transport. *Proceedings of the Royal Society B: Biological Sciences* **2005**, *272*, 1557-1560.
20. Corno, A.F.; Kocica, M.J.; Torrent-Guasp, F. The helical ventricular myocardial band of Torrent-Guasp: potential implications in congenital heart defects. *European journal of cardio-thoracic surgery* **2006**, *29*, S61-S68.
21. Nasiraei-Moghaddam, A.; Gharib, M. Evidence for the existence of a functional helical myocardial band. *American Journal of Physiology-Heart and Circulatory Physiology* **2009**, *296*, H127-H131.
22. Stalder, A.F.; Frydrychowicz, A.; Russe, M.F.; Korvink, J.G.; Hennig, J.; Li, K.; Markl, M. Assessment of flow instabilities in the healthy aorta using flow‐sensitive MRI. *Journal of Magnetic Resonance Imaging* **2011**, *33*, 839-846.
23. Vasava, P.; Jalali, P.; Dabagh, M. Computational Study of Pulstile Blood Flow in Aortic Arch: Effect of Blood Pressure. *In World Congress on Medical Physics and Biomedical Engineering, September 7-12, 2009, Munich, Germany* **2009**, 1198-1201.
24. Shahcheraghi, N.; Dwyer, H.A.; Cheer, A.Y.; Barakat, A.I.; Rutaganira, T. Unsteady and three-dimensional simulation of blood flow in the human aortic arch. *Journal of biomechanical engineering* **2002**, *124*, 378-387.
25. Linde, T.; Hamilton, K.F.; Navalon, E.C.; Schmitz-Rode, T.; Steinseifer, U. Aortic root compliance influences hemolysis in mechanical heart valve prostheses: an in-vitro study. *The International journal of artificial organs* **2012**, *35*, 495-502.
26. Vennemann, B.M.; Rösgen, T.; Carrel, T.P.; Obrist, D. Time-resolved micro PIV in the pivoting area of the triflo mechanical heart valve. *Cardiovascular engineering and technology* **2016**, *7*, 210-222.
27. Bruecker, C.; Steinseifer, U.; Schröder, W.; Reul, H. Unsteady flow through a new mechanical heart valve prosthesis analysed by digital particle image velocimetry. *Measurement Science and Technology* **2002**, *13*, 1043.
28. Gallegos, R.P.; Rivard, A.L.; Suwan, P.T.; Black, S.; Bertog, S.; Steinseifer, U.; Armien, A.; Lahti, M.; Bianco, R.W. In-vivo experience with the Triflo trileaflet mechanical heart valve. *The Journal of heart valve disease* **2006**, *15*, 791-799.
29. Raffel, M.; Willert, C.E.; Scarano, F.; Kähler, C.J.; Wereley, S.T.; Kompenhans, J. *Particle image velocimetry: a practical guide.*; Springer: 2018.
30. Bruecker, C.; Althaus, W. Study of vortex breakdown by particle tracking velocimetry (PTV). *Experiments in fluids* **1992**, *13*, 339-349.
31. Althaus, W.; Bruecker, C.; Weimer, M. Breakdown of slender vortices. In *Fluid Vortices*, Springer: 1995; pp. 373-426.